ISSN 1024-8560, Atmospheric and Oceanic Optics, 2019, Vol. 32, No. 5, pp. 506–510. © Pleiades Publishing, Ltd., 2019.
Russian Text © The Author(s), 2019, published in Optika Atmosfery i Okeana.

OPTICS OF STOCHASTICALLY-HETEROGENEOUS MEDIA

Passive Optical Monitoring of Wind Conditions and Indication of Aircraft Wakes Near Airport Runways

A. L. Afanasiev[a], *, V. A. Banakh[a], **, and D. A. Marakasov[a], ***

[a] *V.E. Zuev Institute of Atmospheric Optics, Siberian Branch, Russian Academy of Sciences, Tomsk, 634055 Russia*

**e-mail: afanasiev@iao.ru*

***e-mail: banakh@iao.ru*

****e-mail: mda@iao.ru*

Received March 7, 2019; revised March 29, 2019; accepted April 5, 2019

Abstract—Wind speed and atmospheric turbulence near an airport runway were measured using a passive optical method, which is based on the correlation analysis of turbulent distortions of distant objects under observation. An optical path was set up in the region of the ground section of a descent glidepath near the beginning of the runway. After an aircraft passed above the line of sight of the measuring device, significant wind speed spikes and increased turbulence in the aircraft wake were detected against the background of a moderate crosswind. The results confirm the practical applicability of this method for instrumental detection of the presence or absence of vortex wakes over an airfield. This information can be useful in the assessment of the safe intervals in air traffic flow-management.

Keywords: crosswind, turbulence, aircraft vortex, air transport safety, passive optical monitoring

DOI: 10.1134/S1024856019050026

INTRODUCTION

An aircraft wake is a restricted disturbance of an atmospheric airmass, which can last for a long time, is unpredictable, and is extremely dangerous for other aircraft. Prevention of aircraft funnelling is one of the most important problems of modern aviation [1]. The total length of the vortex wake is several kilometers and depends on the state of the atmosphere, the aerodynamic and flight configuration of an aircraft, its flight mass, speed, and altitude. The effect of the wake is especially significant when small and medium aircraft follow larger ones. During take-off and landing, because of the special wing configuration, a maximal lift force is created, which also strongly disturbs the air.

Funneling is accompanied by strong turbulence due to strong turbulence in an airmass, which can result in complete loss of control of an aircraft. There have been many aviation accidents, often with tragic consequences, caused by the wake effect. The prevention of such situations is an urgent problem in modern large airports due to the intensity of traffic. An aircraft wake is extremely dangerous in a transparent atmosphere where the wake is invisible, especially during take-off or landing, due to the restricted possibilities for maneuver at low altitudes.

Air traffic controllers predict the presence of a wake during air traffic flow-management and maintain time intervals sufficient for dispersion or wind deflection of the air disturbed from the glidepath, taking into account the actual meteorological conditions. However, the complex dependences the lifetime of the turbulence, its evolution, and trajectory on the meteorological and aircraft parameters and aircraft flight path make the direct instrumental detection of this phenomenon an important problem to be solved.

Lidars have recently come into use for controlling wake turbulence in the glide zone [2–5]. However, these devices are quite complex and expensive and their use is limited to a small number of airports.

Transmission methods based on the statistical analysis of fluctuations of optical radiation propagating in a turbulent atmosphere are simpler techniques for measurement of wind and turbulence [6, 7]. A method based on the analysis of intensity fluctuations (scintillations) of transmitted radiation due to turbulence was used for wind speed estimation in [8]. The use of scintillometers on a runway showed that wake detection is possible in nighttime with relatively weak turbulence. In the daytime, when the turbulence level increases, the turbulence intensity fluctuations are saturated and the sensitivity of the device to vortex wakes falls sharply along paths quite short in comparison with runways [8].

In this work, we present the passive optical monitoring results of the wind situation at the Tolmachevo airport, Novosibirsk. Measurements were performed using a passive optical meter (POM) prototype, which allows estimating wind speed along paths up to 3 km

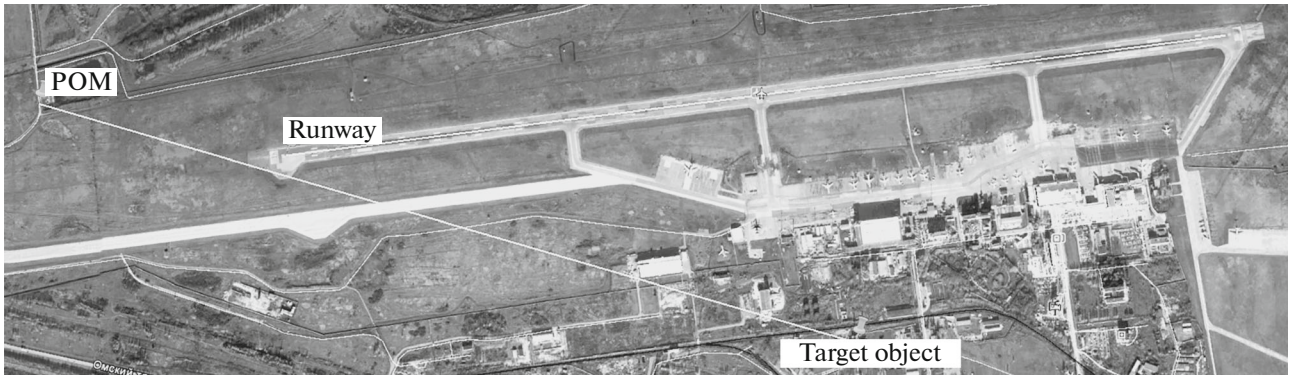

Fig. 1. Orientation of the POM optical path with respect to the runway.

long, including under conditions of strong optical turbulence [9]. An approach to wind speed and atmospheric turbulence estimation based on the phenomenon of jitter of incoherent images of distant objects [10] is implemented in the prototype design. This approach is free from limitations related to the intensity fluctuation saturation. An important feature of the method and device is complete absence of any sources of artificial electromagnetic radiation, which is especially important in airports. POM allows remote real-time measurements of crosswinds and the structure parameter of the refractive index of air C_n^2, which characterizes the power of optical turbulence.

The experiments were designed to use POM to study the possibility of detecting wakes near an airport runway during the take-off and landing of passenger aircraft.

MEASUREMENT ORGANIZATION AND TECHNIQUE

In view of the instrumentation positioned at the airport, chimneys defined against the sky and located at a distance $L = 3100$ m from the POM point were selected as a target. Figure 1 shows the orientation of the optical path along which the crosswind speed and the structure parameter of the air refractive index were measured. The angle between the measuring path and the runway was 23°, i.e., the wind component close to the runway-transverse direction was recorded (at an angle of 67°).

The optical part of the prototype of the video digital crosswind speed meter is shown in Fig. 2. During the measurements, a plot of the wind measured in real-time is displayed on a computer monitor; the current crosswind speed and the correlation function are also displayed.

During the measurements, more than 40 landings of aircraft were recorded; their glidepaths passed directly above the POM measuring path. The landing of an aircraft and the time point of intersection of its trajectory and the line of sight were video-recorded to determine the exact time of aircraft overflight. Figure 3 exemplifies the landing of an aircraft as it flies over the target chimneys. The receiving lenses of the binocular optical system of the POM, which form the image of the selected object for further computer processing and wind speed estimation, are seen in the foreground. Lines show the direction to the target. An image fragment used by POM is shown in the inset.

The wind speed was measured according to the V-shaped scheme, where both channels of an optical system are aimed at the same contrast object. The edge of a chimney was chosen as such an object; it gave a well-distinguished vertical border between the dark and bright parts of the image. The total illumination intensity was calculated in each channel at times t_j, followed by the video frame frequency:

$$P(t_j) = \sum_{l,m=0}^{N-1} I_{lm}(t_j) \quad (1)$$

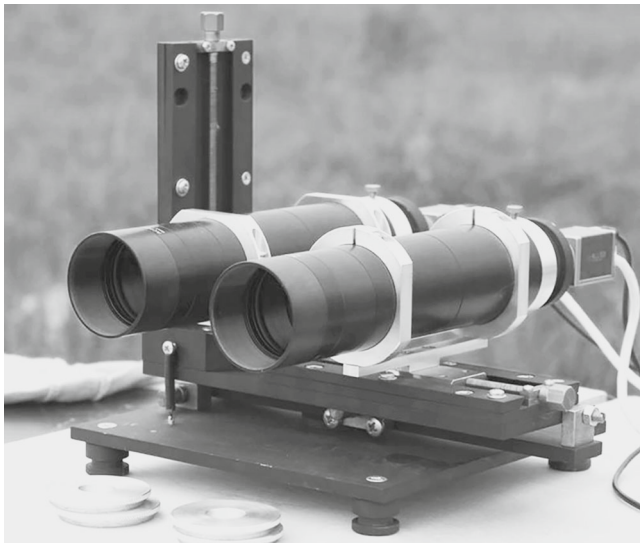

Fig. 2. Passive optical meter.

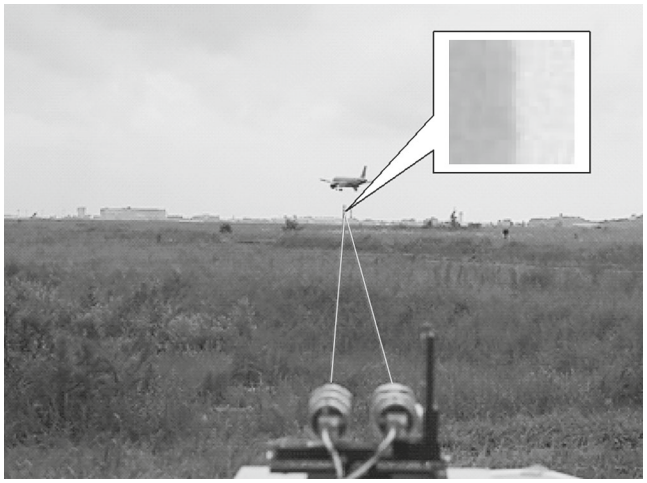

Fig. 3. Instant of aircraft flight over the POM line of sight during landing.

as well as the coordinates of the energy centroids (EC) of images of $N \times N$ pixels in size:

$$\left.\begin{matrix} d_x(t_j) \\ d_y(t_j) \end{matrix}\right\} = \frac{1}{P(t_j)} \sum_{l,m=0}^{N-1} \left\{\begin{matrix} l - N/2 \\ m - N/2 \end{matrix}\right\} I_{lm}(t_j). \quad (2)$$

Due to the specificity of the image regions selected, the horizontal displacements of the EC (d_x) are of higher information content than vertical ones (d_y). Just the horizontal displacement and the noise power were used to estimate the integral values of atmospheric parameters.

The correlation processing of the series was carried out in real-time using the following algorithm. The duration of the statistical averaging interval was set ($T_0 = 16$ s). In this interval, the average noise power and the dispersion of the EC horizontal coordinate in each channel were calculated, as well as the cross-correlation function (CCF) of the series of horizontal displacements in the right and left channels. The averaging interval length selected is sufficient to form the CCF with a clearly distinguishable maximum [11]. The shift τ of the maximum along the abscissa was recalculated into the integral wind speed

$$V = \frac{D}{2\tau}, \quad (3)$$

where D is the space between the POM lenses.

To calculate the structure parameter C_n^2, the ECG shift should be recalculated into the image shift. The equations for the vertical boundary of a homogeneously illuminated object with a constant background intensity derived in [12] were used for the calculation:

$$I(\mathbf{r}) = (I_s - I_0)\chi(x - X_0) + I_0,$$

where $\chi(x)$ is the Heaviside function [13]; X_0 is the horizontal coordinate of the boundary (in pixels); I_0 is the background intensity; and I_s is the intensity in the object image.

During the POM adjustment, the boundary position was selected at the image center, $X_0 = N/2$. The EC horizontal coordinate depends on the image shift ρ_x at $X_0 = N/2$ as

$$d_x - \langle d_x \rangle = \frac{1}{2}\left(\frac{I_s - I_0}{I_s + I_0}\right)^2 \rho_x. \quad (4)$$

The object illumination can noticeably change during long (several minutes and more) continuous measurements. In particular, if the intensity I_s in the object image exceeds the threshold of the receiving array $I_\text{m} = 2^{12} - 1$, I_s should be replaced to I_m in Eq. (4). Those situations were traced without analyzing the structure of images obtained from the measurements; only I_0 and I_s values found from the first frame and the illumination power $P(t_j)$ in the current frame were used. The critical power was defined as

$$P_\text{cr} = \frac{I_\text{m}}{I_s} P(t_0). \quad (5)$$

If this power is exceeded, I_m is used instead of I_s in Eq. (4).

Let us note that this correction is insignificant when estimating the wind, since the proportionality of the EC and image shifts is preserved in any case; hence, the CCF maximum shift remains constant, only its amplitude changes. However, to determine the integral C_n^2 value, the image jitter variance is used [14]:

$$C_n^2 = \frac{\Theta^2 a^{1/3}}{1.1L} \sigma_d^2, \quad (6)$$

where $a = 0.025$ m is the POM lens radius; Θ is the angle which corresponds to one image pixel; and $\sigma_d^2 = \sigma_{d_x}^2 + \sigma_{d_y}^2 = 2\sigma_{d_x}^2$ is the image shift variance. In this case, the variation in the coefficient in Eq. (4) is important.

MEASUREMENT RESULTS

Figure 4 shows real time passive optical estimates of the integral crosswind speed along the path. The times of takeoffs and landings are marked on the time axis. The images of aircraft which produce a specific wake are shown above the corresponding times. High wind speed spikes caused by the wake passage are seen on the background of a light crosswind (~1–3 m/s) at the times of aircraft overflights. Undisturbed (natural) values of the crosswind are restored some time after the wake is carried away from the line of sight of the POM.

Figure 5 shows a measurement episode with a very weak crosswind (<1 m/s). The curves of simultaneous variations in the wind speed (top) and the structure parameter C_n^2 are shown. Under weak wind, a double

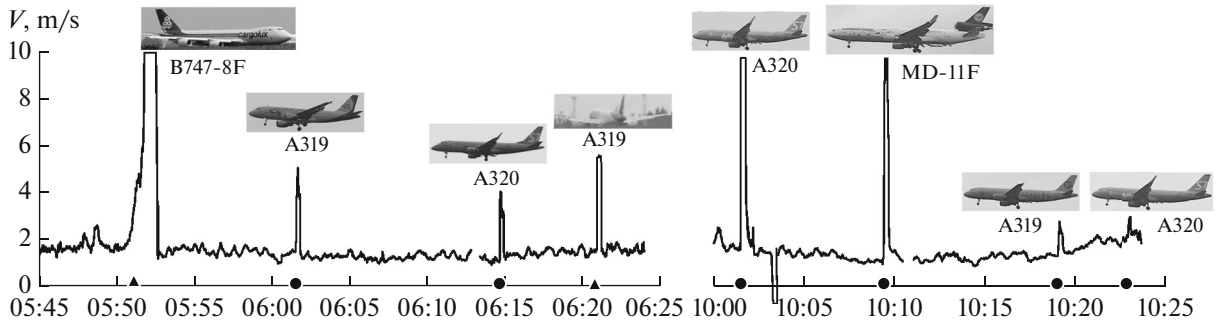

Fig. 4. Integral crosswind speed along the optical path below the glide path near the beginning of runway (▲ corresponds to takeoff, and ●, to landing).

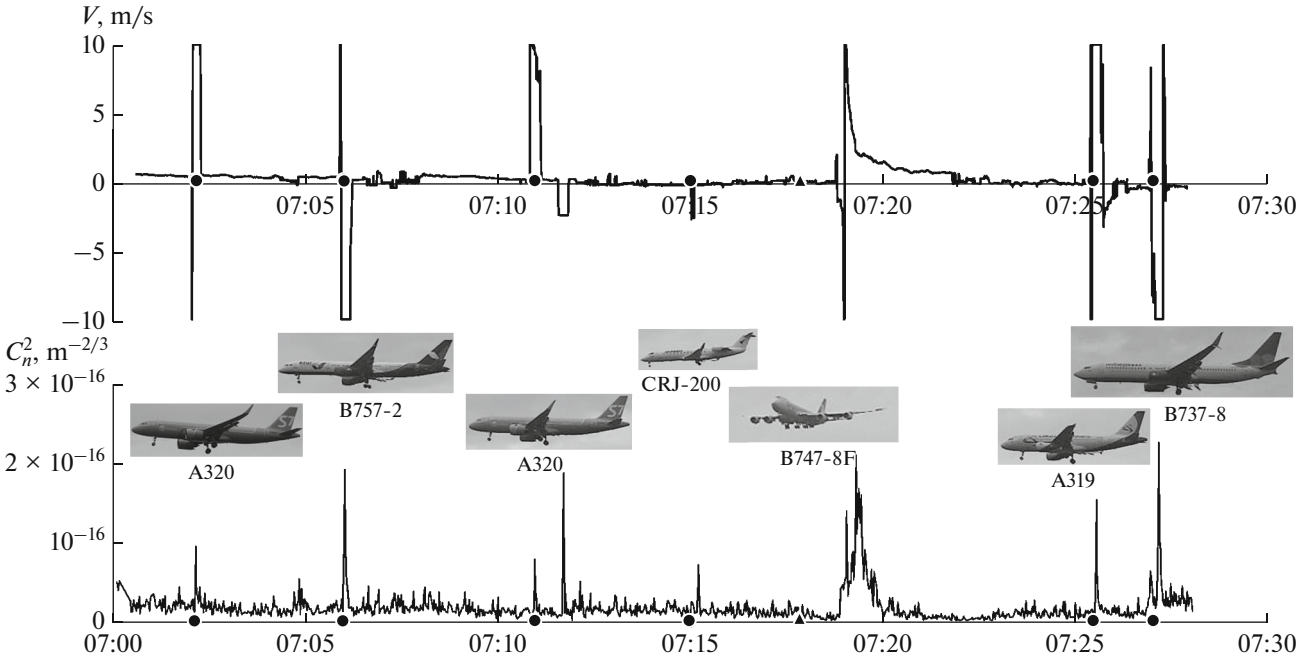

Fig. 5. Episode of simultaneous measurements of the crosswind speed (top) and C_n^2 (bottom) which shows the vortex character of the wakes with a sharp change in the speed direction and turbulence strengthening (▲ corresponds to takeoff, and ●, to landing)

speed spike is observed, with a sharp change in the spike direction. This behavior reflects the vortex nature of the wake. It is obvious that the wake effect is the most dangerous under these conditions, with slow carryover of the disturbed air from the glidepath and abrupt changes in the direction.

According to Figs. 4 and 5, the wind speeds are in the range ±10 m/s. This is explained by the fact that the maximal modulus of the speed V, measured by POM, is determined by the minimal measurable delay τ of the CCF maximum, which is limited by the time interval of sampling (interframe gap) $1/f$. Due to the POM specification (frame rate $f = 250$ Hz and lens spacing $D = 10$ cm), the speed assessments in this case were limited to $V_{max} = 10$ m/s. The real velocity spikes could slightly exceed this value during the measurements. This limitation is insignificant for the demonstration of sharp wind gusts, indicating the presence of a wake on the line of sight. It can be overcome by means of decreasing the spacing of POM lenses and increasing the video frame rate.

Characteristic spikes, several times higher that the background values, are also seen on the C_n^2 curve in Fig. 5 at the time of wake passage. The relatively small amplitude of the bursts ($\sim 2 \times 10^{-16}$ m$^{-2/3}$) is explained by the fact that the path integral characteristic is measured, while the disturbances occur on a relatively small local segment of the path. Estimates of the structural characteristics in the vortex wake taking account

of the approximate sizes of the disturbance zone and the linearity of accumulation of fluctuations of the angle of arrival along the path [14], give values $C_n^2 \sim 10^{-13}$–10^{-12} m$^{-2/3}$, which is close to the measurement results [8].

The capability of POM to estimate C_n^2 along with the crosswind speed is an additional advantage of the method. Simultaneous monitoring of these two different physical characteristics can improve the reliability of detection of the disturbed airflow in the line of sight. The above examples show the pronounced response of the POM to the appearance of a disturbed air flow in the region of a runway with sharply different values of the local velocity and intensity of turbulence.

CONCLUSIONS

The formation of powerful vortex air flows near a runway at the airport during takeoff and landing of aircraft requires safe intervals in air traffic. Since the lifetimes and spatial localization of such turbulent perturbations are difficult to predict, their immediate detection by technical means is an urgent problem. In order to study the possibility of detecting aircraft wakes on airport territory, a passive optical method based on the correlation processing of turbulent distortions of binocular images of distant topographic objects for measuring the crosswind and atmospheric turbulence has been implemented.

The results confirm the practical applicability of this method in the rapid remote detection of the presence or absence of aircraft wakes in the runway region and the glide zone of an aircraft. The passive optical measurements can be particularly useful under conditions of a transparent atmosphere and quiet weather, where the wakes have shown spatiotemporal stability and are barely detectable by other means. Minimization of traffic intervals based on real-time measurements can significantly increase the airport capacity without building additional runways.

FUNDING

The work was supported by the Russian Academy of Sciences (Fundamental Research Project no. AAAA-A17-117021310149-4) and, partly, by the Russian Foundation for Basic Research (project no. 18-42-700005 r_a).

CONFLICT OF INTEREST

The authors declare that they have no conflicts of interest.

REFERENCES

1. V. J. Rossow, "Lift-generated vortex wakes of subsonic transport aircraft," Prog. Aerospace Sci. **35** (6), 507–660 (1999).
2. M. Harris, R. I. Young, F. Kopp, A. Dolfi, and J.-P. Cariou, "Wake vortex detection and monitoring," Aerospace Sci. Technol. **6** (5), 325–331 (2002).
3. I. N. Smalikho and V. A. Banakh, "Estimation of aircraft wake vortex parameters from data measured with 1.5 mcm coherent Doppler lidar," Opt. Lett. **40** (14), 3408–3411 (2015).
4. I. N. Smalikho, V. A. Banakh, F. Holzäpfel, and S. Rahm, "Estimation of aircraft wake vortex parameters from array of radial velocities measured by a coherent Doppler lidar," Opt. Atmos. Okeana **28** (8), 742–750 (2015).
5. N. Smalikho, V. A. Banakh, and A. V. Falits, "Measurements of aircraft wake vortex parameters by a Stream Line Doppler lidar," Atmos. Oceanic Opt. **30** (6), 588–595 (2017).
6. R. S. Lawrence, G. R. Ochs, and S. F. Clifford, "Use of scintillations to measure average wind across a light beam," Appl. Opt. **11** (2), 239–243 (1972).
7. V. E. Zuev, V. A. Banakh, and V. V. Pokasov, *Optics of Atmospheric Turbulence* (Gidrometeoizdat, Leningrad, 1988) [in Russian].
8. D. Van Dinther, O. K. Hartogensis, and A. A. M. Holtslag, "Runway Wake vortex, crosswind, and visibility detection with a scintillometer at Schiphol airport," Bound.-Lay. Meteorol. **157** (3), 481–499 (2015).
9. A. L. Afanasiev, V. A. Banakh, E. V. Gordeev, D. A. Marakasov, A. A. Sukharev, and A. V. Falits, "Verification of a passive correlation optical crosswind velocity meter in experiments with a Doppler wind lidar," Atmos. Ocean. Opt. **30** (6), 574–580 (2017).
10. A. L. Afanasiev, V. A. Banakh, and A. P. Rostov, "Estimation of the integral wind velocity and turbulence in the atmosphere from distortions of optical images of naturally illuminated objects," Atmos. Oceanic Opt. **29** (5), 422–430 (2016).
11. A. L. Afanasiev, V. A. Banakh, and D. A. Marakasov, "Comparative assessments of the crosswind speed from optical and acoustic measurements in the surface air layer," Atmos. Ocean. Opt. **31** (1), 43–48 (2018).
12. A. L. Afanasiev, V. A. Banakh, D. A. Marakasov, and A. P. Rostov, "Field tests of a passive optical meter of the structure characteristic of refractive index," Proc. SPIE—Int. Soc. Opt. Eng. **10466** (2017). https://doi.org/10.1117/12.2287118
13. *Handbook of Mathematical Functions with Formulas, Graphs and Mathematical Tables*, Ed. by M. Abramowitz and I.A. Stegun (U.S. Government Printing Office, Washington, 1972).
14. V. P. Lukin, "Adaptive system for the formation of laser beams in the atmosphere by use of incoherent images as reference sources," Atmos. Ocean. Opt. **26** (4), 345–351 (2013).

Translated by O. Ponomareva